Aalborg Universitet

AALBORG UNIVERSITY

DENMARK

Surface entropy of rare gas clusters

Prasalovich, S.; Hansen, K.; Kjellberg, M.; Popok, Vladimir; Campbell, Eleanor E.B.

Surface entropy of rare-gas clusters

S. Prasalovich, K. Hansen,[a] M. Kjellberg, V. N. Popok, and E. E. B. Campbell
Department of Physics, Gothenburg University, SE-41296 Gothenburg, Sweden

Abundances of Ar_N^+ and Xe_N^+ clusters produced in a supersonic expansion source are inverted to find relative dissociation energies. The values around the shell and subshell closings at $N=55$, 71, and 147 differ from theoretical values derived from ground-state energies of Lennard-Jones clusters. A significant part of the difference can be accounted for by the conformational entropies of surface atoms and vacancies. © *2005 American Institute of Physics.* [DOI: 10.1063/1.2008948]

I. INTRODUCTION

An important aspect of the nonmonotonous approach of matter in the growth from a single atom to bulk sizes is the shell structure, which was first discovered in rare-gas clusters.[1] The enhanced stability of certain cluster sizes ($N=55,147$, etc.) was inferred from the high abundance of these sizes in mass spectra. The stability pattern was interpreted in a very simple picture, viz., representing the atoms as spheres and packing these while optimizing the number of nearest-neighbor interactions. This successfully explained the presence of the so-called magic numbers, which are understood as geometric shells with the symmetry of Mackay icosahedra.[2] Several other magic numbers were also observed. Consistent with the interpretation of the shell closings, these were explained as subshell closings, where single faces and vertices were covered with atoms.

The mere presence of shell closings does not give any information on the magnitude of the energies involved and does not allow any comparison between theory and experiment beyond statements about the relative experimental "magic" nature of peaks. A quantitative comparison requires knowledge of the binding energies of the clusters. It is possible to extract those from the mass spectra under some assumptions,[3] with the restriction that only relative values can be found. This is particularly interesting because the magic numbers, as defined by local high abundances, do not always coincide with the shell closings of packing shells. In a number of cases these two differ by plus or minus one atom and are even absent in some cases, e.g., $N=55$ for Ar clusters. Extracting binding energies will allow one to judge to what extent these discrepancies are effects of the methods used or reflect structural properties of the clusters.

II. EXPERIMENT

The experimental data used in this work consists of time-of-flight (TOF) mass spectra of Ar_N^+ and Xe_N^+ clusters, produced in a pulsed supersonic expansion source with typical stagnation pressures of 90 and 40 bar, respectively. The clusters were ionized with electron impact a few millimeters downstream from the nozzle with electron energies of 90 eV.

After skimming and accelerating in a pulsed field to 4 keV, the clusters entered a 0.7-m linear TOF mass spectrometer and were detected with a dual channel-plate detector. The flight time between production and entry into the acceleration region of the TOF mass spectrometer was 0.9 ms for argon and 1.6 ms for xenon clusters. After acceleration, the clusters flew for an additional $5-150$ μs, depending on their mass, before being detected. The optimized mass resolution was $N/\Delta N \approx 200$. For a more detailed description of the apparatus see Ref. 4.

The measured mass distributions depend on a number of source working parameters, such as the backing pressure, ion-focusing conditions, and ionization current. The setup does not allow a simultaneous optimization of the resolution of all masses, probably due to the long flight time from the source to the mass spectrometer. The spectra are therefore recorded with the optimum resolution and intensity in different mass regions and only the central, optimized region is used in the analysis. The individual spectra have mass distributions with a broad envelope upon which several rapidly varying abundance anomalies are superposed (Fig. 1), similar to the spectra found in the literature.[5–7] The background in the spectra was not negligible and some remarks concerning background subtraction are given below. The various, resolution- and intensity-optimized spectra were analyzed independently. To show the full scale of detected masses, the resolved parts of the spectra were connected together and plotted as one data set in Fig. 2. The mass range covered is
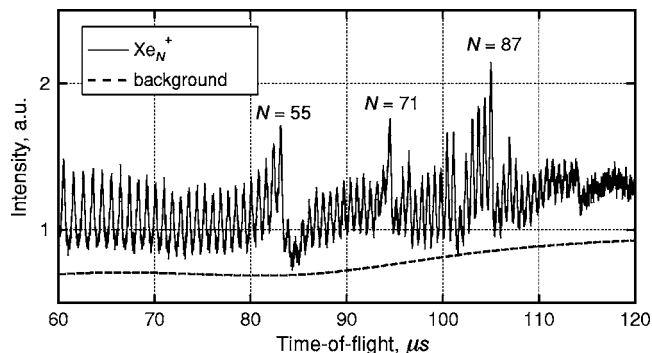

FIG. 1. Abundance spectrum for Xe clusters. The dashed line is the background which was removed. The data for $N>110$ were not used for the evaluation.
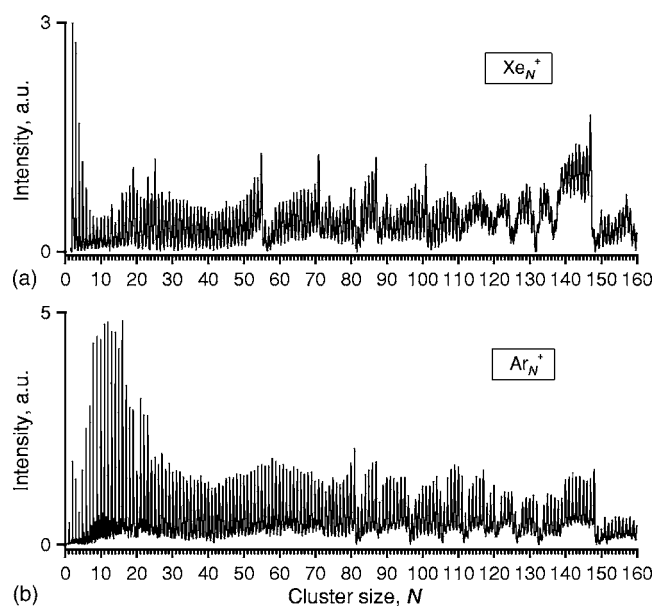
FIG. 2. Abundance spectra of (a) Xe and (b) Ar clusters. Obtained from fitting together regions of different mass spectra optimized for maximum intensity and resolution (see text for details).

from monomers to $N=160$ for both cluster materials. Based on the similarity between these spectra and the ones from the literature on supersonic sources,[5–7] we conclude that the spectra are indeed typical and no further systematic study of the influence of the source conditions or the ionization parameters was made.

III. ANALYSIS

Measured cluster spectra will, apart from the kinetics of the formation, also be shaped by the subsequent decay in the beam. Local size-to-size variations reflect the postproduction evaporation and are expected to be insensitive to the global shape of the distribution. These therefore contain information about the size-to-size variations of the evaporative rate constants. Provided the frequency factors for the rate constants, ω_N, are known, the connection between the abundance spectra and the cluster binding energies are the evaporative activation energies.[3] We will make the reasonable assumption that there are no reverse activation barriers present. Then the activation energies are the dissociation energies, D_N, i.e., the differences between ground-state energies of clusters N and $N+1$. We will give a brief derivation of the relation between the abundances and binding energies for small clusters found in Ref. 3, and expand on relevant points.

With a proper definition of the temperature, the evaporation rate constant can be written as an Arrhenius expression:

$$k_N = \omega_N \exp\left(\frac{-D_N}{k_B(T_N - D_N/2C_v)}\right), \tag{1}$$

where T is the microcanonical temperature,[8] C_v is the heat capacity, and ω_N is the frequency factor which is vastly exceeding reciprocal experimental times, but which will be left unspecified at this point. The term $D_N/2C_v$ is Klots' finite

heat bath correction.[9] Solving for the internal energy in terms of the rate constant one has

$$E_N = \frac{C_{v,N}D_N}{k_B \ln(\omega_N/k_N)} + \frac{D_N}{2} - E_{N,0}, \tag{2}$$

where the zero-point energy $E_{N,0}$ is defined by the caloric curve $E_N = C_{v,N}T_N - E_{N,0}$. Using Eq. (2) with the highest value of k_N possible in the ensemble at time t, $k_N = 1/t$,[10] gives the upper limit of the energy distribution,

$$E_N(\max) = \frac{C_{v,N}D_N}{k_B \ln(\omega_N t)} + \frac{D_N}{2} - E_{N,0}. \tag{3}$$

The value of t is the above-mentioned 0.9 ms for argon clusters and 1.6 ms for xenon clusters.

The high-energy cutoff in Eq. (2) has the consequence that there is also a low-energy cutoff,

$$E_N(\min) \approx E_{N+1}(\max) - D_{N+1}, \tag{4}$$

where we have disregarded the small kinetic-energy release E_{kin}. The difference between the two energies, $E_N(\max) - E_N(\min)$, is on the order of one dissociation energy, but with important corrections when D_N and D_{N+1} are different.

The low-energy cutoff is present if the clusters have evaporated at least one atom. The evidence that this is the case is rather strong. Experiments on argon clusters involving ionization, with and without subsequent photoabsorption, do not show any significant difference between the two different types of abundance spectra.[11] The measured mass loss after absorption of visible and near-infrared (NIR) photons is at least five atoms for cluster size 10, and increases with size. The abundance spectra for argon and krypton clusters were also found to be invariant to changes in source conditions,[12] in complete agreement with our experience. These facts are not difficult to accept, given the huge ratio between the ionization energy and the typical dissociation energy. The same conclusion was reached in Ref. 13.

For small clusters, the two energy cutoffs are fairly sharp, and we can write the abundance as the integral of the energy distribution, $g(E)$, between these two limits:

$$I_N = \int_{E_N(\min)}^{E_N(\max)} g(E)dE. \tag{5}$$

The function $g(E)$ represents a smooth distribution related to the details of the cluster formation. One important consequence of the two energy limits, $E_N(\max)$ and $E_N(\min)$, is that at a specific time, only clusters of a certain size will have a given excitation energy. Excitation energy is thus mapped onto the cluster size distribution. Furthermore, this mapping is dense. For every excitation energy there is a cluster of a certain size with that energy. Since g is a smooth function we can consider g as a function of size, i.e., $g=g(N)$ instead of energy, $g=g(E)$. If we denote quantities that are smoothly varying with cluster size by a tilde, we have

$$\tilde{I}_N = g(N)\tilde{D}_N. \tag{6}$$

We can now write the relative abundances in Eq. (5) as

$$I_N = \int_{E_N(\text{min})}^{E_N(\text{max})} g(E)dE = \frac{\widetilde{I}_N}{\widetilde{D}_N} \int_{E_N(\text{min})}^{E_N(\text{max})} dE. \tag{7}$$

Using the integration limits derived above we have

$$I_N = \frac{\widetilde{I}_N}{\widetilde{D}_N}\left(\frac{D_N + D_{N+1}}{2} + C_{v,N}\frac{D_N}{k_B \ln(\omega_N t)} \right.$$
$$\left. - C_{v,N+1}\frac{D_{N+1}}{k_B \ln(\omega_{N+1}t)} \right), \tag{8}$$

where we have left out the difference between the E_0's, which is on the order of the vibrational frequency. Equivalently,

$$\frac{I_N}{\widetilde{I}_N} = \frac{1}{\widetilde{D}_N}\left(\frac{D_N + D_{N+1}}{2} + C_{v,N}\frac{D_N}{k_B \ln(\omega_N t)} \right.$$
$$\left. - C_{v,N+1}\frac{D_{N+1}}{k_B \ln(\omega_{N+1}t)} \right). \tag{9}$$

A background in the raw data can potentially distort this relation. The effect was estimated by arbitrarily adding a constant equal to the average peak integral to all integrated peaks. This changed the size-to-size amplitude of the variation of the dissociation energies, calculated as described below, by a factor of 2 (for the case where $\omega_N = \omega_{N+1}$), but had no other effect.

In order to proceed, $\widetilde{I}_N$ must be determined. There is some freedom in the choice of this function. It should not vary too rapidly with N, because in that case the interesting abundance variations will disappear in the ratio $I_N/\widetilde{I}_N$, and it should vary sufficiently rapidly to remove the slow variations of I_N, i.e., the envelope of the abundance distribution. We have chosen a Gaussian with a running width:

$$\widetilde{I}_N \equiv \frac{\sum_{N'} I_{N'} \exp(-(N'-N)^2/0.015N^2)}{\sum_{N'} \exp(-(N'-N)^2/0.015N^2)}, \tag{10}$$

where the sum runs over all masses in the spectrum.

IV. RESULTS

The result of the mass spectra normalization procedure using Eq. (10) is shown in Fig. 3. As can be seen from comparison with Fig. 2, the procedure preserves the relative magnitude of the local variations in the abundances with the parameters chosen. Furthermore, we see that the renormalized abundances from all the spectra, with different average cluster sizes, agree well. This is a strong argument in favor of the assumption that the local variations in the spectra are due to the properties of the clusters and not the details of the production.

Equation (9) is a first-order difference equation and requires one boundary value. It was found that the equation was stable when solved numerically from the high-N part of the spectrum towards low N's. The result of the inversion is shown in Fig. 4. We have used $C_v = 3N-7$ for the heat capacity, which corresponds to one less than the canonical heat capacity of $3N-6$ harmonic oscillators,[8] and the value
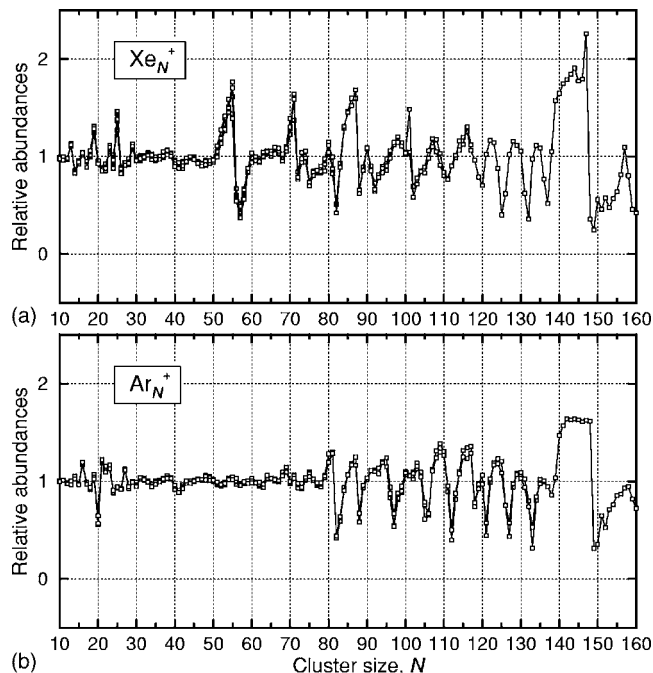
FIG. 3. Abundance spectra divided by the corresponding smooth spectra for (a) Xe and (b) Ar clusters.

$\ln(\omega_N t) = 31$ for all Ar clusters.[14] The relatively large value is due to the long time interval elapsed between production/ionization and detection. One must expect a variation in the frequency factor due to the increasing surface area with increasing cluster size. The effect of this is small, however, because $\omega_N t$ is very large compared with unity, and we will not consider them further. For Xe, the value of 34 is used, which includes the longer flight time between the source and the TOF and the higher evaporation rate due to the higher mass of the Xe atom.[15]
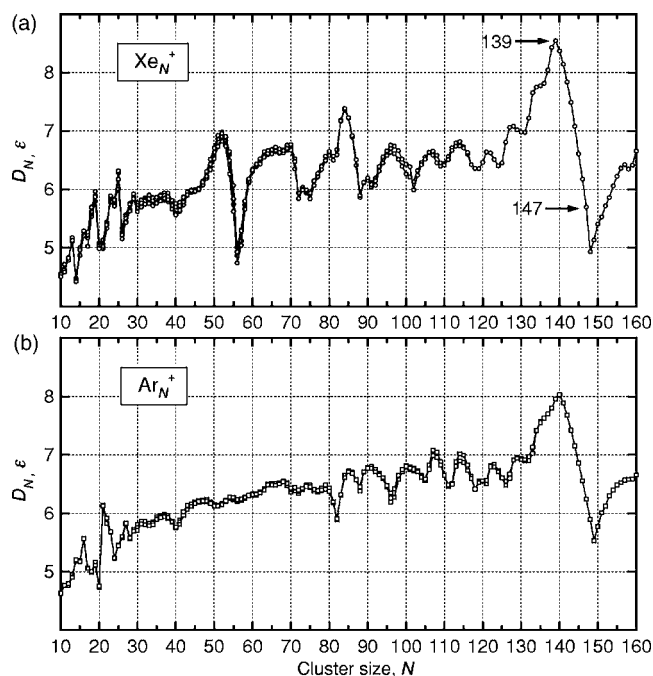
FIG. 4. Dissociation energies for (a) Xe_N^+ and (b) Ar_N^+, calculated with Eq. (9) and $W_N = 1$ and scaled with the liquid drop model. The energy ε unit refers to the scaled Lennard-Jones potential.

There are two noteworthy aspects of Fig. 4. The first is that the amplitude of the dissociation energy variations does not follow the same trend as the local abundance variations. Whereas the extremes in dissociation energy tend to decrease when the size increases, this is not the case for the abundance spectrum. The reason for this difference is clear from Eq. (9), which shows that the effect is caused by the heat capacity which is roughly proportional to size, and hence has a magnifying effect for the abundances at high N.

The other aspect is the different location of the high abundances and the high dissociation energies. Effectively, application of Eq. (9) shifts the magic number downwards in mass from, e.g., $N=147$ in the abundance spectrum to $N=139$, which is the locally highest point in the curve of the dissociation energy. This contradicts the naive intuition that the largest abundances should represent the largest dissociation energies. It also seems to contradict the calculations in, e.g., Ref. 16 of ground-state energies of neutral van der Waals clusters. The reason for the failure of the intuition is the importance of the second term in Eq. (9), which associates large abundances with large *changes* in dissociation energy. A systematic error in C_v or $\ln(\omega_N t)$ will mainly cause a change in the *amplitude* of the variations in the dissociation energy around the mean as long as the error varies smoothly with N.

At first sight these results seem to jeopardize the otherwise well-substantiated interpretation of the abundances in terms of geometric shell closings, or alternatively, to undermine trust in the assumptions on which Eq. (9) is based. We will suggest an explanation which supports both and, in fact, strengthens them, and shows that the data are indeed consistent with the configurations and, partly also, the energies calculated in Ref. 16.

In the application of Eq. (9) it was tentatively assumed that the frequency factor varied smoothly and only little with size. This is true if the thermal properties of the two clusters that enter the reaction scheme, parent and daughter, are smoothly varying with size. A smooth size variation is destroyed, e.g., by the presence of size-specific surface effects. These are most easily understood quantitatively by application of the detailed balance equation for the atomic evaporation constant. This is proportional to the ratio of the level densities of the daughter, $\rho_{N-1}(E-D_N)$, and the parent cluster, $\rho_N(E)$.[15]

$$k(E) = \omega_N' \frac{\rho_{N-1}(E-D_N)}{\rho_N(E)}. \tag{11}$$

The frequency factor ω_N' is expected to depend only weakly on size (and energy) and can be set to a constant, which is the procedure used in Ref. 3. Frequently, the ratio of level densities can be converted directly into a Boltzmann-type factor, which is also the procedure used above. The conversion is determined by the caloric curves, i.e., the $E(T)$ relations, of the clusters. But the caloric curve only determines the level density up to a multiplicative constant. This is easy to verify for the canonical ensemble, where the excitation energy is given by the logarithmic derivative of the partition function with respect to the reciprocal temperature, β:

$$\langle E \rangle = -\frac{d \ln Z}{d\beta}, \tag{12}$$

when it is remembered that the partition function is

$$Z = \int \rho(E) e^{-\beta E} dE. \tag{13}$$

The logarithmic derivative in Eq. (12) cancels any multiplicative constant in the level density.

Hence, without changing the caloric curves, the ratio of level densities in Eq. (11) may contain the ratio of two otherwise unobserved multiplicative factors on the level density. Such factors arise from the configurational entropy of the clusters. For a certain cluster size, N, the ground state may allow a number, W_N, of distinct, but energetically degenerate, configurations. A similar observation has been made in Ref. 17 to explain the variations in the melting temperatures of sodium clusters. We can factor out the vibrational level density, $\rho_{v,N}(E)$, as $\rho_N(E)=W_N\rho_{v,N}(E)$. The frequency factor will be modified by the factor W_{N-1}/W_N:

$$\omega_N = \omega_N' \frac{W_{N-1}}{W_N}. \tag{14}$$

The numbers W_N can be calculated once the ground-state configurations of the clusters are known.

The degeneracies will be caused by the different configurations of atoms at the surface, hence the name surface entropy for the quantity $S_N = k_B \ln W_N$. The justification for the term is even more clearly seen if Eq. (11) is rewritten slightly:

$$
\begin{aligned}
k(E) &= \omega_N' \frac{\rho_{N-1}(E-D_N)}{\rho_N(E)} = \omega_N' \frac{W_{N-1}\rho_{v,N-1}(E-D_N)}{W_N\rho_{v,N}(E)} \\
&\approx \omega_N' \frac{W_{N-1}}{W_N} \exp\left(-\frac{D_N}{k_B T}\right) \\
&= \omega_N' \exp\left(-\frac{D_N - T(S_{N-1} - S_N)}{k_B T}\right),
\end{aligned}
$$

where for simplicity of notation we have used $T = T_N - D_N/2C_v$. Recalling that D_N is the difference between two (negative) ground-state energies, $D_N = E_{gs,N-1} - E_{gs,N}$, we have the suggestive form of the activation energy

$$D_N \rightarrow (E_{gs,N-1} - TS_{N-1}) - (E_{gs,N} - TS_N). \tag{15}$$

Although the two parentheses are reminiscent of free energies, it is clear that the identification is not perfect, because the energies refer to ground-state properties and the surface entropy is only a small part of the total entropy of the clusters. In fact, the overwhelming part of the entropy is given by the level densities themselves and not by the minor corrections imposed by the surface entropy. With this caveat, we nevertheless find the expression in Eq. (15) instructive.

In the practical application of this correction we have used the binding energies and configurations calculated in Ref. 16. The assumption underlying this choice is that the measured clusters take these structures. This is not trivial since the calculated structures refer to neutral clusters and the measured clusters are positively charged. It has the virtue

that it conforms with the accepted interpretation of the abundance spectra in terms of icosahedral shell closings. A different choice of configuration will lead to a different entropy, which will then give a different binding energy. The smooth part of the dissociation energy is calculated in the liquid drop approximation $E_N = AN - BN^{2/3}$, where E_N is the total binding energy of cluster size N, A is the bulk binding energy per atom, and B is proportional to the surface tension. A fit of the theoretical values of the equivalent relation $E_N/N = A - B/N^{-1/3}$ gives $A = 8.09$ and $B = 11.67$. The energy unit refers to the scaled Lennard-Jones potential $V_{LJ} = \varepsilon(r^{-12} - 2r^{-6})$. The entropies were calculated by inspection of the ground-state configurations in Ref. 16. The values used are given in Table I. The values for $N = 148 - 150$ are estimated by analogy to the $N = 56 - 58$ cases. In Ref. 17 W_N was calculated by considering all sites on the surface of the cluster to be equivalent. This is probably justified considering the higher temperatures of the clusters in these experiments, and there is no contradiction to our calculated values, also because the cluster materials are different (sodium versus rare-gas atoms).

To compare the result of the inversion of Eq. (9) with the theoretical values, we have multiplied the output, $D_N/\tilde{D}_N$, with the liquid drop energy, using the A and B parameters above. The result is shown in Fig. 5, together with the result of the $W_N = 1$ inversion, also scaled with the liquid drop values. The figure shows regions around high-abundance cluster sizes. In most cases these are also expected shell or subshell closings. All the experimental data sets have been merged, averaging them with equal weight. The difference in D's between different data sets is small. For, e.g., $N = 55$ (Xe) the standard deviation on the mean value amounts to 2.6%. The full list of all the calculated binding energies for Ar and Xe, together with the theoretical dissociation energies from Ref. 16, are given in Table I.

At the low-size end ($N = 15 - 35$), where the effect of the surface entropy is small (the dissociation energies calculated with and without taking this quantity into account are almost similar), there is a marked difference between the dissociation energies expected from geometric packing and the experimental results. The deviation is most pronounced for Ar, where the two curves are almost uncorrelated. For Xe, the expected subshell closing at $N = 19$ is found in the data, even with an amplitude D_{20}/D_{19}, which is very close to the expected value. The high value at $N = 25$, however, is uncorrelated with the packing shell structure. The overall discrepancy between the data and the packing shell structure, and between the two different cluster types, suggests that the energetics in this mass region is influenced strongly by the charge state of the clusters. This effect must be expected to disappear with increasing size, which indeed seems to be the case (see below).

A previous study of binding energies of Xe_N^+ clusters used the metastable fraction in a reflectron time-of-flight mass spectrometer to extract the relative dissociation energies for sizes $N = 11 - 39$.[18] The results are not identical to ours. This is partly due to relatively slow variations with size, which the present analysis is not able to capture. The local variations, however, are in fairly good agreement above $N = 19$, also with respect to the amplitude. The main dis-

agreement arises at sizes $N = 15 - 18$ where the variations in Ref. 18 exceed ours by a large margin and where the ratio of the dissociation energies of $N = 16$ and $N = 17$ reaches almost a factor of 3 (see Fig. 3 of Ref. 18). The discrepancy between the two sets of results for these few sizes is not yet understood.

In the region $N = 40 - 60$, which includes the shell closing at $N = 55$, the abundance spectra of Ar differ from those of Xe. Whereas the latter has a strong peak at $N = 55$, the argon spectra are almost without any features in that region. The dissociation energies calculated with $W_N = 1$ are also different, with no size dependence for Ar, but a sizable variation around $N = 55$ for Xe. The Xe values at this shell closing are particularly instructive. The strong peak in the abundance spectrum is converted into a more smoothly increasing dissociation energy when the size is approached from above, and the dissociation energy reaches its maximum four masses below, at $N = 51$. When the finite entropy is included, the picture changes markedly. The smooth approach from the minimum value at $N = 56$ to the maximum at $N = 51$ is replaced by a very abrupt increase from D_{56} to D_{55}, where it almost reaches its maximum. Above the shell closing, minor variations in the D's correlate reasonably well with those expected from the geometric packing, although the amplitudes of these are still significantly smaller in the experimental data. This is also seen in the Ar case, where a small dip at $N = 55 - 56$ also develops. For both Ar and Xe, the effect of the surface entropy is clearly visible and improves the agreement with the packing structure results.

The region $N = 60 - 80$ includes the experimentally strong peak at $N = 71$. Also here, the Xe abundance spectrum shows the largest effect in the inversion when $W_N = 1$. However, once the surface entropy is included, the dissociation energies of Ar and Xe are in much better agreement with each other and with the packing shell structure. It should be noted that the magic number $N = 71$ in the abundance spectra actually corresponds to a locally most stable $N = 70$.

In the region $N = 90 - 110$, the effect of the surface entropy becomes very pronounced and actually dominates the dissociation energy variations. This region is midshell and the calculation of the entropy is not certain for these cluster sizes. An uncertainty which is particularly severe here is that the close-lying isomers are not included. The dissociation energies in this mass region are therefore less certain than the rest.

The region $N = 130 - 150$ includes the strong shell closing at $N = 147$. The Ar and Xe spectra show similar behavior in this region and this is also reflected in the calculated dissociation energies. For both spectra there is a reasonable agreement between packing shell and experimental dissociation energies, in the region around $N = 135$. Between $N = 137$ and 146, the agreement is less satisfactory. At $N = 147$, the agreement is again better, with the data reproducing the abrupt decrease in D between 147 and 148. The magnitude of the jump is more than half the value expected from Ref. 16. Furthermore, there is no ambiguity in the data as to the precise magic number; both Xe and Ar clusters show a strong decrease in dissociation energies when going from $N = 147$ to $N = 148$.

TABLE I. N—cluster size, W_N—number of equal atomic arrangements in the outer shell of the icosahedron calculated from the structures given in Ref. 16, ΔE_N—difference in binding energies of $(N-1)$ and (N) clusters (Ref. 16), and D_N, D_N^*—dissociation energies calculated in this work, without and with entropy correction for Ar and Xe clusters, respectively. The energy unit ε refers to the scaled Lennard-Jones potential.

N	W_N	ΔE_N	$D_N(\text{Ar})$	$D_N^*(\text{Ar})$	$D_N(\text{Xe})$	$D_N^*(\text{Xe})$
13	1	6.36	4.95	5.19	5.14	5.33
14	20	3.52	5.17	4.85	4.45	4.21
15	30	4.48	5.19	5.16	4.94	4.92
16	60	4.49	5.58	5.43	5.26	5.12
17	30	4.50	5.05	5.10	5.18	5.21
18	12	5.21	5.01	5.16	5.59	5.75
19	12	6.13	5.14	5.23	5.90	5.99
20	60	4.52	4.81	4.61	5.04	4.85
21	60	4.51	6.13	6.12	5.04	5.04
22	60	5.13	5.84	5.82	5.38	5.36
23	30	6.03	5.67	5.81	5.85	5.99
24	120	4.51	5.25	5.01	5.78	5.54
25	60	5.02	5.45	5.52	6.19	6.27
26	20	5.94	5.58	5.80	5.24	5.42
27	60	4.56	5.82	5.64	5.50	5.34
28	60	4.95	5.57	5.55	5.69	5.67
29	30	5.77	5.70	5.84	5.87	5.99
30	60	4.70	5.75	5.63	5.68	5.58
31	60	5.30	5.85	5.84	5.76	5.75
32	30	6.05	5.82	5.97	5.81	5.94
33	60	5.21	5.79	5.68	5.85	5.74
34	30	5.20	5.81	5.96	5.81	5.95
35	120	5.71	5.90	5.64	5.81	5.58
36	60	6.07	5.94	6.05	5.86	5.96
37	120	5.21	5.95	5.79	5.88	5.73
38	60	6.10	5.93	6.03	5.86	5.94
39	12	6.90	5.86	6.19	5.76	6.06
40	60	5.22	5.78	5.51	5.67	5.43
41	60	5.29	5.83	5.83	5.71	5.71
42	60	5.74	5.99	5.99	5.82	5.82
43	60	6.09	6.09	6.09	5.93	5.93
44	120	5.32	6.12	5.97	5.97	5.83
45	120	6.10	6.17	6.12	5.98	5.94
46	30	6.90	6.20	6.46	6.00	6.23
47	120	5.33	6.20	5.90	6.10	5.83
48	60	6.19	6.21	6.30	6.25	6.33
49	20	6.89	6.18	6.38	6.41	6.60
50	60	5.46	6.14	5.91	6.59	6.36
51	30	6.70	6.14	6.25	6.80	6.90
52	20	6.98	6.16	6.24	6.91	6.97
53	30	6.97	6.22	6.13	6.83	6.72
54	12	7.01	6.26	6.45	6.49	6.64
55	1	7.04	6.25	6.83	5.82	6.30
56	20	4.40	6.23	5.70	4.90	4.52
57	60	4.70	6.23	6.02	5.17	5.01
58	20	6.04	6.27	6.51	5.73	5.93
59	30	5.36	6.30	6.25	6.15	6.10
60	60	6.14	6.33	6.19	6.33	6.21
61	30	6.13	6.34	6.49	6.41	6.55
62	60	5.35	6.37	6.24	6.48	6.36
63	120	6.14	6.42	6.27	6.58	6.44
64	60	6.13	6.50	6.63	6.62	6.75
65	120	5.30	6.49	6.34	6.64	6.49
66	60	6.13	6.49	6.62	6.67	6.79
67	60	6.21	6.50	6.50	6.65	6.64
68	120	6.14	6.54	6.37	6.65	6.49
69	60	6.33	6.50	6.62	6.72	6.83

TABLE I.   (*Continued.*)

N	W_N	ΔE_N	$D_N(\mathrm{Ar})$	$D_N^*(\mathrm{Ar})$	$D_N(\mathrm{Xe})$	$D_N^*(\mathrm{Xe})$
70	12	7.17	6.40	6.75	6.71	7.04
71	12	6.46	6.42	6.47	6.45	6.49
72	120	5.17	6.38	5.92	5.87	5.49
73	60	6.27	6.42	6.55	6.01	6.12
74	60	6.12	6.47	6.47	5.96	5.96
75	120	5.13	6.46	6.31	5.90	5.77
76	60	6.14	6.40	6.53	6.12	6.23
77	60	6.29	6.38	6.38	6.25	6.24
78	60	6.22	6.41	6.40	6.38	6.38
79	30	7.13	6.43	6.58	6.52	6.66
80	60	6.27	6.41	6.27	6.62	6.49
81	30	6.26	6.19	6.33	6.54	6.69
82	120	6.21	5.90	5.63	6.64	6.36
83	30	6.37	6.32	6.60	7.18	7.47
84	60	5.73	6.63	6.49	7.37	7.23
85	20	6.40	6.72	6.97	7.22	7.48
86	120	6.33	6.69	6.31	6.91	6.55
87	60	6.71	6.57	6.72	6.46	6.59
88	120	6.84	6.41	6.27	5.88	5.75
89	20	7.12	6.71	7.10	6.12	6.45
90	90	6.38	6.77	6.46	6.18	5.92
91	120	6.38	6.78	6.71	6.08	6.02
92	20	6.37	6.73	7.13	6.13	6.47
93	120	5.69	6.67	6.30	6.36	6.04
94	120	6.39	6.60	6.59	6.51	6.50
95	120	6.38	6.46	6.45	6.61	6.60
96	120	6.24	6.27	6.26	6.70	6.69
97	120	6.80	6.32	6.31	6.70	6.68
98	120	6.87	6.60	6.59	6.59	6.58
99	30	7.12	6.72	7.03	6.46	6.72
100	60	6.37	6.81	6.66	6.35	6.23
101	30	6.37	6.77	6.93	6.30	6.44
102	60	5.87	6.75	6.61	6.06	5.95
103	120	6.38	6.72	6.57	6.28	6.15
104	60	6.38	6.63	6.77	6.44	6.57
105	120	6.23	6.58	6.43	6.53	6.40
106	120	6.79	6.79	6.77	6.63	6.62
107	120	6.85	7.03	7.02	6.62	6.61
108	60	7.12	7.00	7.15	6.52	6.64
109	120	6.38	6.86	6.69	6.43	6.29
110	60	6.38	6.66	6.79	6.43	6.55
111	60	6.28	6.47	6.47	6.54	6.53
112	60	6.81	6.50	6.50	6.69	6.69
113	120	6.83	6.84	6.68	6.77	6.62
114	60	7.13	6.96	7.10	6.78	6.91
115	60	6.80	6.93	6.93	6.72	6.71
116	12	7.17	6.78	7.14	6.62	6.94
117	120	5.47	6.62	6.13	6.42	5.99
118	60	6.49	6.41	6.54	6.36	6.48
119	60	6.65	6.54	6.53	6.35	6.35
120	120	5.60	6.55	6.39	6.47	6.32
121	120	6.80	6.53	6.51	6.64	6.62
122	120	7.12	6.81	6.79	6.62	6.60
123	60	6.86	6.82	6.95	6.51	6.62
124	60	7.12	6.72	6.71	6.40	6.39
125	60	6.38	6.61	6.59	6.45	6.44
126	120	6.05	6.51	6.35	6.81	6.65
127	30	7.13	6.64	6.91	7.06	7.33
128	120	6.85	6.91	6.58	7.08	6.77
129	60	7.13	6.95	7.08	7.02	7.13

TABLE I.   (*Continued.*)

N	W_N	ΔE_N	$D_N(Ar)$	$D_N^*(Ar)$	$D_N(Xe)$	$D_N^*(Xe)$
130	120	6.81	6.93	6.74	6.98	6.81
131	30	7.17	6.91	7.19	6.97	7.23
132	120	5.60	6.93	6.60	7.22	6.90
133	20	6.98	7.08	7.46	7.65	8.03
134	20	6.97	7.41	7.40	7.75	7.74
135	1	8.29	7.56	8.31	7.77	8.48
136	12	7.18	7.63	7.04	7.81	7.26
137	30	7.18	7.70	7.46	8.04	7.81
138	20	7.18	7.80	7.89	8.43	8.51
139	60	7.18	7.96	7.65	8.54	8.24
140	60	7.18	8.03	7.99	8.37	8.33
141	12	7.18	7.88	8.27	8.14	8.50
142	60	7.18	7.68	7.25	7.84	7.44
143	30	7.18	7.42	7.55	7.49	7.60
144	20	7.18	7.15	7.22	7.08	7.13
145	30	7.18	6.86	6.74	6.61	6.50
146	12	7.19	6.56	6.72	6.17	6.31
147	1	7.19	6.24	6.73	5.70	6.10
148	60	4.61	5.89	5.10	4.93	4.32
149	60	5.62	5.53	5.48	5.13	5.09
150	20	6.62	5.77	5.93	5.41	5.54

V. DISCUSSIONS

The results of the above analysis merit several comments. First of all, we see that the inclusion of the surface entropy removes several discrepancies between the magic numbers of, in particular, Ar clusters and the high-stability species expected from an analysis of Lennard-Jones clusters. The inclusion of the term also brings the dissociation energies of Xe and Ar clusters in closer agreement than would be inferred from a direct comparison of the respective abundance spectra. Also, the absolute magnitude of the size-to-size variations are in reasonable agreement with the theoretical binding energies. In this connection the inclusion of the surface entropy is essential.

There are several effects which have not been considered in the analysis here, some of which will have quantitative consequences. Of these, the presence of low-energy isomers is one of the most important. In the calculation of the surface entropy it was assumed that only the ground-state degeneration counted. But since the clusters decay thermally, the finite excitation energy should allow other low-energy configurations to be populated and, in principle, these should also be included in the entropy calculation. One may proceed with this in two ways: one may calculate the effect in numerical simulations or one may also approach the problem from the experimental side. With the reasonable assumption that the isomers of the shell closings are too high in energy to be populated, it will be possible to set the entropy of these special sizes to zero. This allows the calculation of entropies at smaller sizes, up to a single additive constant (the surface entropy of the shell closing plus one atom), by requiring that the energies correspond to the Lennard-Jones energies.

Before this can be done, one would need to address the question of the heat capacity of the clusters, as well as the effect of the charge. The heat capacity used here refers to classical, or high-temperature, harmonic oscillators. The excitation energy per vibrational degree of freedom of the clusters in the present experiments is expected to be above, but of similar magnitude as the vibrational quantum. Deviations from classical harmonic oscillator heat capacities and the corresponding level densities will modify the rate constants, and consequently, the energy content of the clusters,[19] calculated in Eq. (2).

The charge will modify thermal properties, and more importantly, influence the dissociation energies so the simple Lennard-Jones estimate is no longer valid. One reason is that the atomic polarizabilities of the two elements (Ar and Xe) are different, as are their radii. Another is that the quantum-mechanical behavior of the charge is different for the two elements. For Xe clusters the ionic core was found to be either a trimer or a tetramer, with both of these represented in cluster sizes in the range relevant here, in theoretical work[20,21] and experimentally corroborated.[22,23] For argon clusters the charge was calculated to be localized on two, three, or four atoms[20,24,25] (up to $N=22$) or three atoms[26] (up to $N=27$). The structure with dimeric core was found to have much higher energies compared with the ground-state energies of trimers and tetramers, however, it could become competitive when cluster size increases ($N > 20$).[24,25] We expect the effects of charge to be strongest for small clusters, consistent with the observations here, and when it comes to abundance spectra, also to be different for the two elements. The charge will deform the cluster from the neutral shape and cause a partial or, for small clusters, a complete lifting of the geometric degeneracy.

A direct comparison between experimental dissociation energies obtained for Ar_n^+ clusters in the present work and theoretical relative binding energies from Ref. 26 can be done, as shown in Fig. 6. The difference in amplitude be-
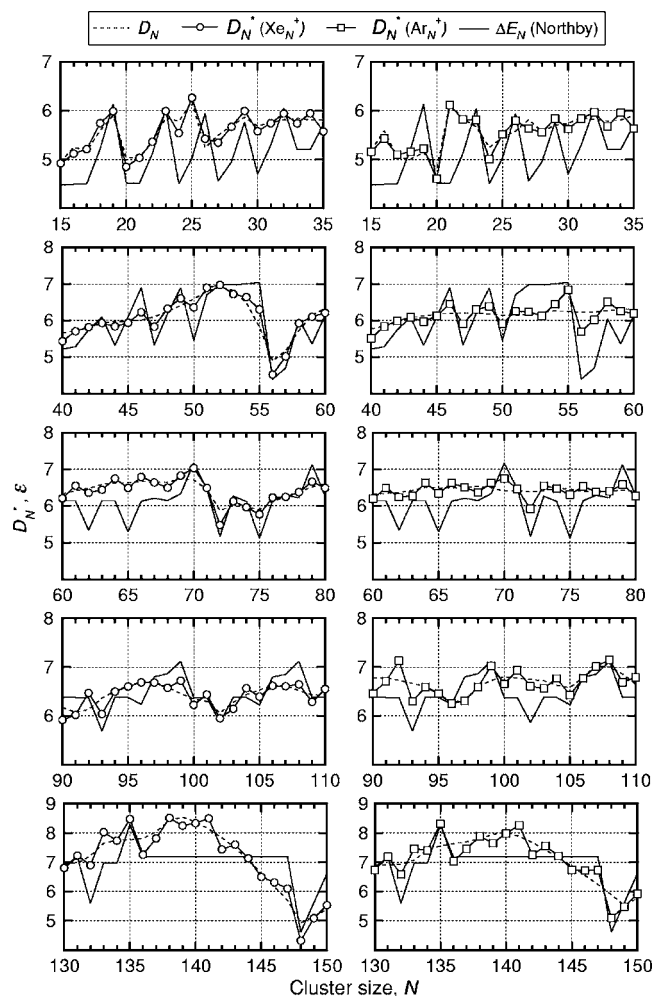
FIG. 5. Dissociation energies calculated from the experimental data with the procedure described in the text. D_N—dissociation energies without the surface entropy included, D_N^*—dissociation energies from experimental data with surface entropies included, and ΔE_N—binding energies according to Ref. 16. The energy unit ε refers to the scaled Lennard-Jones potential.

tween the two sets of data, especially pronounced for smaller sizes, may be due to the liquid drop approximation applied to our data in order to scale the energies with cluster size. The general trend of the curves agrees to some extent. For $N = 13$, 16, and 19 the curves peak on both theoretical binding energy and experimental dissociation energy (with entropy correction included). It is also important to mention here that similar maxima are predicted by the theory for neutral clusters according to the closed-shell model.[16] Besides this agreement, the theory for charged clusters fails to reproduce the experimental maxima at $N = 21$ and 23 and predicts a peak at $N = 25$, which is not observed in our experiments for Ar_n^+ clusters. The importance of charge is therefore very difficult to determine from such a comparison and additional studies are required.

The theoretical binding energies by Paška *et al.* for Xe_N^+ from Ref. 27 show some of the similar features as the theoretical results for Ar_N^+, in particular, the high average value for small cluster sizes. But the trends seem to agree better with the experimental results (see Fig. 7). As for larger clusters, the relative amplitude in the variation is larger than the
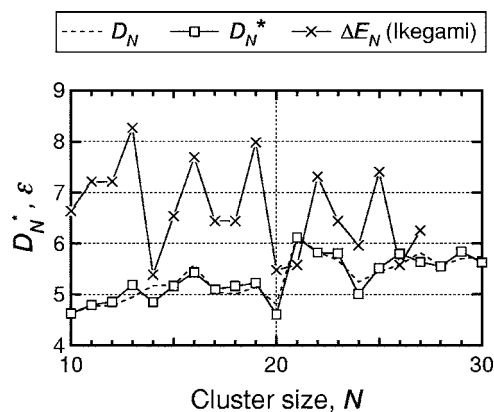

FIG. 6. Dissociation energies (D_N—before the entropy correction, D_N^*—corrected due the configurational entropy) calculated from the experimental data as compared with the computed binding energies (ΔE_N) from Ref. 26 for Ar_N^+ clusters. The energy unit ε refers to the scaled Lennard-Jones potential.

experimental results by a factor of about 2. These authors identify a pentamer as the charged core in the high size range.

Among other approximations of the analysis presented here is the use of a completely classical picture. This is reflected in the vibrational level density of the clusters, as already mentioned. But it also has consequences for the calculation of the surface entropy. The assumption used here is that different configurations are distinguishable states, and, e.g., symmetry numbers can be set equal to unity. The treatment of the atoms in the cluster as classical and distinguishable particles is consistent with the standard treatment of rare-gas clusters. This is most likely a good approximation, but the transition from a quantum-mechanical description to a classical one raises questions that deserve future attention.

The use of surface entropy also requires that the atoms in the unfilled shell are mobile. We expect this is indeed the case. The reason is that the activation energy for motion on the surface is smaller than the one for evaporation, because the number of nearest neighbors for a mobile atom is always larger (two or more) than that of an evaporated atom (zero). This causes the migration to happen with a much higher rate
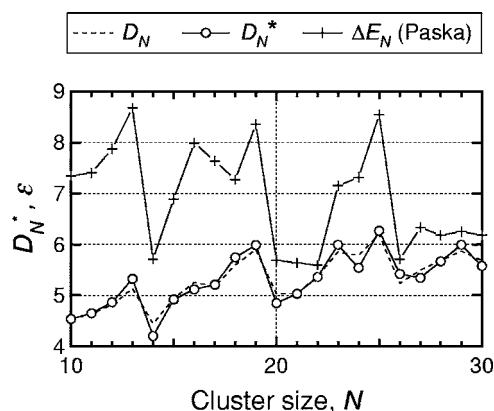

FIG. 7. Dissociation energies as in Fig. 6, but for Xe_N^+ clusters. The theoretical curve is from Ref. 27. Experimental points below $N \approx 10$ are not represented correctly because of the small width used to calculate $\tilde{I}_N$ from Eq. (10).

than the evaporation, and the cluster will consequently sample the different conformations efficiently on the time scale of evaporation. This is the criterion for including these states into the total level density.

VI. CONCLUSIONS

We have inverted experimental abundance spectra of Ar and Xe clusters to obtain the relative dissociation energies for the size range $N=10-150$. The inversion with a size-independent frequency factor of the rate constant gave a relatively smooth curve for D_N, where shell and subshell closings are barely discernible. The inversion associates strong abundance anomalies with strong *changes* in dissociation energies. Inclusion of the entropy, associated with the number of different ground-state isomers, improved the agreement with the dissociation energies calculated for Lennard-Jones clusters. In particular, the shell closings are easier to identify as strong and abrupt decreases of the dissociation energy between N and $N+1$. The amplitudes of the drops are smaller than theoretically predicted, but comparable to those. The agreement with Lennard-Jones clusters is poor only for the smallest cluster sizes, $N=10-20$, and inclusion of the surface entropy has very little consequence for those. In this region, the two cluster materials have different magic numbers, suggesting that these binding energies are influenced strongly by the positive charge. The analysis hinges on a knowledge of the geometrical structure of the clusters, which at present are derived from simulations on neutral clusters. A full picture of the energies and structures of rare-gas clusters requires further work to elucidate the effects of this and other approximations.

[1] O. Echt, K. Sattler, and E. Recknagel, Phys. Rev. Lett. **47**, 1121 (1981).
[2] A. I. Mackay, Acta Crystallogr. **15**, 916 (1962).
[3] K. Hansen and U. Näher, Phys. Rev. A **60**, 1240 (1999).
[4] V. N. Popok, S. V. Prasalovich, M. Samuelsson, and E. E. B. Campbell, Rev. Sci. Instrum. **73**, 4283 (2002).
[5] W. Miehle, O. Kandler, T. Leisner, and O. Echt, J. Chem. Phys. **91**, 5940 (1989).
[6] P. G. Lethbridge and A. J. Stace, J. Chem. Phys. **89**, 4062 (1988).
[7] P. Scheier and T. D. Märk, Int. J. Mass Spectrom. Ion Processes **76**, 11 (1987).
[8] J. U. Andersen, E. Bonderup, and K. Hansen, J. Chem. Phys. **114**, 6518 (2001).
[9] C. E. Klots, J. Chem. Phys. **83**, 5854 (1985).
[10] J. Gspann, Z. Phys. D: At., Mol. Clusters **3**, 143 (1986).
[11] N. E. Levinger, D. Ray, M. L. Alexander, and W. C. Lineberger, J. Chem. Phys. **89**, 5654 (1988).
[12] A. Ding and J. Hesslich, Chem. Phys. Lett. **94**, 54 (1983).
[13] J. M. Soler, J. J. Saenz, N. Garcia, and O. Echt, Chem. Phys. Lett. **109**, 71 (1984).
[14] K. Hansen and E. E. B. Campbell, Int. J. Mass. Spectrom. **233**, 215 (2004).
[15] K. Hansen, Philos. Mag. B **79**, 1413 (1999).
[16] J. A. Northby, J. Chem. Phys. **87**, 6166 (1987).
[17] H. Haberland, T. Hippler, J. Donges, O. Kostko, M. Schmidt, and B. von Issendorff, Phys. Rev. Lett. **94**, 035701 (2005).
[18] S. Wei, Z. Shi, and J. Castleman, J. Chem. Phys. **94**, 8604 (1991).
[19] C. Predescu, P. A. Frantsuzov, and V. A. Mandelshtam, J. Chem. Phys. **122**, 154305 (2005).
[20] P. J. Kuntz and J. Valldorf, Z. Phys. D: At., Mol. Clusters **8**, 195 (1988).
[21] M. Amarouche, G. Durand, and J. P. Malrieu, J. Chem. Phys. **88**, 1010 (1988).
[22] H. Haberland, B. von Issendorff, T. Kolar, H. Kornmeier, C. Ludewigt, and A. Risch, Phys. Rev. Lett. **67**, 3290 (1991).
[23] T. Laarmann, A. Kanaev, K. von Haeften, H. Wabnitz, R. von Pietrowski, and T. Møller, J. Chem. Phys. **116**, 7558 (2002).
[24] F. Calvo, J. Galindez, P. Paska, D. Hrivnak, R. Kalus, and F. X. Gadéa, Comput. Phys. Commun. **145**, 126 (2002).
[25] H.-U. Böhmer and S. D. Peyerimhoff, Z. Phys. D: At., Mol. Clusters **11**, 239 (1989).
[26] T. Ikegami, T. Kondow, and S. Iwata, J. Chem. Phys. **98**, 3038 (1993).
[27] P. Paška, D. Hrivňák, and R. Kalus, Chem. Phys. **286**, 237 (2003).